Ultrawideband Antenna Distortion Compensation

Wasim Q. Malik, *Member, IEEE*, Christopher J. Stevens, and David J. Edwards

***Abstract*—The radiation characteristics of ultrawideband (UWB) antennas vary with frequency, introducing directionally asymmetric bandwidth reduction and waveform dispersion. In this paper, we develop a simple technique to alleviate the distortion due to nonisotropically dispersive antennas, and use indoor channel measurements to verify its performance. The approach is based on multipath direction estimation and therefore involves antenna arrays. We show that antenna distortion can enhance sensor localization ambiguity and introduce errors in its estimate. Antenna compensation mitigates this effect, significantly improving the location estimation accuracy. We further demonstrate that antenna compensation helps reduce the small-scale fading artifacts that arise due to the antennas, thus reducing the channel spatial variability and delay spread. Our technique can also aid empirical channel characterization by providing antenna-independent propagation data.**

***Index Terms*—Antenna, array, direction-of-arrival (DOA) estimation, distortion, sensor localization, ultrawideband (UWB).**

I. Introduction

In RECENT years, ultrawideband (UWB) systems have gained prominence due to many promising applications such as indoor multimedia communications and sensor networks [1]. The Federal Communications Commission (FCC) in the US has allocated the 3.1–10.6 GHz spectrum for UWB emissions [2]. According to the current FCC specification, a UWB signal has a bandwidth of between 0.5–7.5 GHz [2], as opposed to only a few KHz for conventional narrowband systems. The antennas and propagation aspects of UWB systems therefore differ significantly from those of narrowband systems [1], [3]. The design of practical antennas that radiate efficiently over an ultrawide bandwidth continues to be a challenging problem [4]. Apart from wideband matching and radiation efficiency, another problem arising from antenna distortion is signal dispersion. UWB antenna radiation patterns vary significantly with frequency, leading to a direction-specific distortion of UWB waveforms [5]–[7]. An indoor UWB channel is characterized by a large number of incident multipath components (MPCs), with three-dimensional scattering and large angular spreads [1]. As a result, individual MPCs experience nonuniform distortion due to the antenna, determined by their directions-of-departure (DODs) and directions-of-arrival (DOAs). In an impulse radio UWB system with a correlation-based receiver [8], this nonuniform multipath distortion can result in large and unpredictable correlation mismatches at the receiver, consequently degrading the system performance. Similarly, signal distortion is experienced due to multiple-antenna arrays that often suffer from beam pattern variations with frequency. While our discussion in this paper will be limited to a single antenna element, the proposed technique can be easily extended to array distortion and its compensation.

In this paper, we investigate the effects of antenna distortion with emphasis on sensor location estimation and communications channel fading. We develop a technique for antenna distortion compensation making use of antenna arrays for multipath direction determination. The proposed compensation technique can improve the performance of wireless sensor localization schemes that rely on DOA estimation [9]. It can also be used to remove antenna artifacts from channel measurement data and to thus obtain antenna-independent channel models. Finally, in a communications application, it can upgrade the link performance by mitigating the small-scale fading introduced due to antennas. We substantiate these claims with the help of antenna and channel measurements, followed by system simulations, and the results prove the efficacy of the proposed technique. In related work [10], we have applied this technique to UWB indoor channel data generated using ray-tracing, with a simulated propagation environment identical to that in this paper, and the results are found to be in close agreement with those reported here.

The rest of this paper is organized as follows. Section II outlines the system model and develops the formalism for the antenna and channel analysis. Section III describes the proposed UWB antenna compensation algorithm. Section IV evaluates the consequent improvement in communications and localization performance, and also quantifies the signal-to-noise ratio (SNR) penalty due to noise enhancement. Finally, the conclusions are drawn in Section IV.

II. System Model

The radiation and reception characteristics of UWB antennas are well understood in literature [1], [4]. An impulse radiating antenna can be modelled as a spatio-temporal linear time invariant filter, with the exciting voltage, $u_t(t)$, as its input parameter and the radiated field as the output parameter. At a far-field distance d in freespace, the co-polar component of the radiated electric field due to a linearly polarized UWB antenna can be expressed as [7], [11], [12]

$$e_t(\theta_t, \phi_t, t) = \frac{K_t}{2\pi dc} b_t(\theta_t, \phi_t, \tau) * \delta(\tau - \tau_p) * \frac{\partial}{\partial t} u_t(t) \quad (1)$$

where $c = 3 \times 10^8$ m/s is the wave velocity in freespace, $\tau_p = d/c$ is the propagation delay, θ_t and ϕ_t are the elevation

Manuscript received December 6, 2006; revised March 1, 2008. Published July 7, 2008 (projected). This work was supported by the ESU Lindemann Trust and the U.K. Engineering and Physical Sciences Research Council under Grant GR/T21769/01.

W. Q. Malik is with the Department of Brain and Cognitive Sciences, Massachusetts Institute of Technology, Cambridge, MA 02139 USA (e-mail: wqm@mit.edu).

C. J. Stevens and D. J. Edwards are with the Department of Engineering Science, University of Oxford, Oxford OX1 3PJ, U.K. (e-mail: christopher.stevens@eng.ox.ac.uk, david.edwards@eng.ox.ac.uk).

Color versions of one or more of the figures in this paper are available online at http://ieeexplore.ieee.org.

Digital Object Identifier 10.1109/TAP.2008.924690

and azimuth transmit directions, $\partial(\cdot)/\partial t$ is the time derivative operator, $u_t(t)$ is the voltage signal at the input terminals of the transmitting antenna, $K_t = \sqrt{Z_0/Z_t}$ with Z_0 and Z_t denoting the freespace impedance and transmit antenna input impedance respectively, $\delta(\cdot)$ is the Dirac delta function and $*$ is the convolution operator. In (1), $b_t(\theta_t, \phi_t, \tau)$ is the co-polar component of the antenna transient response, which forms a Fourier transform pair with the antenna effective height [7].

In accordance with the reciprocity theorem, the voltage signal at the output port of the receiving antenna corresponding to the incident plane wavefield in freespace is [11]

$$u_r(t) = \frac{1}{K_r} b_t(\theta_r, \phi_r, \tau) * e_r(\theta_r, \phi_r, t) \tag{2}$$

where θ_r and ϕ_r are the receive elevation and azimuth angles, $K_r = \sqrt{Z_0/Z_r}$, $e_r(\theta_r, \phi_r, t)$ is the incident electric field, and $b_r(\theta_r, \phi_r, \tau)$ is the transient response of the receiving antenna. For an end-to-end freespace system comprising a pair of such antennas, we can combine (1) and (2) to obtain [7]

$$\begin{aligned} u_r(t) =& \frac{K}{2\pi dc} b_r(\theta_r, \phi_r, \tau) * b_t(\theta_t, \phi_t, \tau) \\ & * \delta(\tau - \tau_p) * \frac{\partial}{\partial t} u_t(t) \end{aligned} \tag{3}$$

where $K = K_t/K_r = \sqrt{Z_r/Z_t}$. In practical radio systems, both antennas usually have the same characteristic port impedance so that $K = 1$ in (3). In this discussion, we are not interested in the time derivative property of the antenna, and therefore define $\partial u_t(t)/\partial t = s(t)$. Also substituting $r(t) = u_r(t)$ for notational uniformity, (3) becomes

$$r(t) = \frac{K}{2\pi dc} b_r(\theta_r, \phi_r, \tau) * b_t(\theta_t, \phi_t, \tau) * \delta(\tau - \tau_p) * s(t).$$

From Fourier theory, in the frequency domain we have

$$R(f) = \frac{K}{2\pi dc} B_r(\theta_r, \phi_r, f) B_t(\theta_t, \phi_t, f) e^{-j2\pi f \tau_p} S(f) \tag{4}$$

where $B_t(\theta_t, \phi_t, f)$ and $B_r(\theta_r, \phi_r, f)$ are the effective transmitting and receiving antenna heights, and $S(f)$ and $R(f)$ are the transmitted and received voltage signals in the frequency domain, respectively. Fig. 1 illustrates this system model.

The above description is based on the double-directional propagation model [13], according to which we can represent the spatio-temporal response of the UWB multipath channel, excluding the antennas, by $h(\theta_t, \phi_t, \theta_r, \phi_r, t)$. Thus, in addition to the multipath gains and delays, the channel applies an angular transformation from the transmitter to the receiver for each MPC, as shown in Fig. 2. In the rest of this paper, we will use $r_h(t)$ to denote the signal received after propagation through the multipath channel, h. Now, we can rewrite (4) in terms of the complex spatio-temporal transfer functions of the channel and antennas in the frequency domain as

$$R_{thr}(f) = A_r(\theta_r, \phi_r, f) H(\theta_t, \phi_t, \theta_r, \phi_r, f) A_t(\theta_t, \phi_t, f) S(f) \tag{5}$$

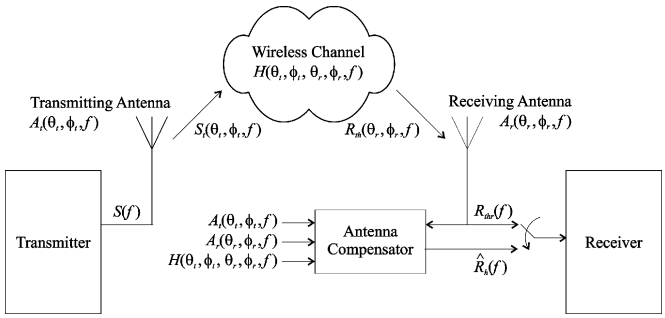

Fig. 1. A wireless communications system with the signal distortion due to directionally asymmetric antenna characteristics in a multipath UWB channel. The received signal, $R_{thr}(f)$, contains the effect of the transmitting and receiving antennas in addition to the physical propagation channel. With the antenna compensator, an estimate of the signal without antenna distortion, $\hat{R}_h(f)$, can be obtained given the knowledge of the antenna directional distortion functions and the multipath directions-of-departure and arrival.

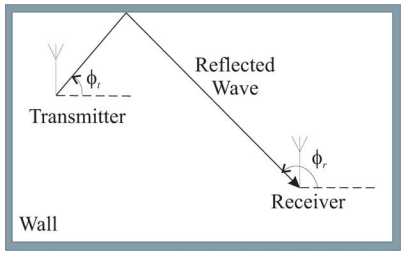

Fig. 2. A two-dimensional representation of the transformation between the azimuth angle-of-departure, ϕ_t, and angle-of-arrival, ϕ_r, during propagation.

where $A_t(\theta_t, \phi_t, f)$ and $A_r(\theta_r, \phi_r, f)$ represent the amplitude transfer functions of the transmitting and receiving antennas, respectively. Note that we use the notation R_{thr} to emphasize that the received signal is distorted by the transmitting and receiving antennas in addition to the channel, $H(\theta_t, \phi_t, \theta_r, \phi_r, f)$. The antenna complex gain, $A_r(\theta_r, \phi_r, f)$, is related to its power radiation pattern, $P_r(\theta_r, \phi_r, f)$, as

$$P_r(\theta_r, \phi_r, f) = |A_r(\theta_r, \phi_r, f)|^2$$

and a similar expression governs the relationship of A_t and P_t. If the two antennas are perfectly isotropic and broadband within the band of interest, $f_l \le f \le f_h$, i.e.,

$$A_t(\theta_t, \phi_t, f) = A_r(\theta_r, \phi_r, f) = 1 \tag{6}$$

then the received signal spectrum in (5) reduces to

$$R_{thr}(f) = H(\theta_t, \phi_t, \theta_r, \phi_r, f) S(f). \tag{7}$$

Real UWB antennas, however, significantly modify the spectrum of the multipath signal depending on its DOD and DOA characteristics, so that (6) is usually not obeyed [4], [7]. We describe this situation in terms of the *composite channel*, including the dispersion due to the multipath scattering and also the transmitting and receiving antennas. The signal

$$S_t(\theta_t, \phi_t, f) = A_t(\theta_t, \phi_t, f) S(f)$$

emitted from the transmitting antenna is then non-isotropic. After propagation through the multipath channel, the signal incident at the receiving antenna can be expressed as

$$R_{th}(\theta_r, \phi_r, f) = H(\theta_t, \phi_t, \theta_r, \phi_r, f) S_t(\theta_t, \phi_t, f).$$

Additional distortion is caused to this signal by the receiving antenna, so that the received signal becomes

$$\begin{aligned} R_{thr}(f) &= A_r(\theta_r, \phi_r, f) R_{th}(\theta_r, \phi_r, f) \\ &= H_{thr}(f) S(f) \end{aligned}$$

where

$$H_{thr}(f) = A_r(\theta_r, \phi_r, f) H(\theta_t, \phi_t, \theta_r, \phi_r, f) \times A_t(\theta_t, \phi_t, f)$$

is the composite channel transfer function.

Our technique facilitates the estimation of the true channel response, H, by compensating for both A_t and A_r, given information on the angular-spectral antenna patterns and multipath propagation. The latter can be obtained using double-directional channel characterization techniques, involving multiple-antenna arrays at both ends of the link.

In the interest of simplicity, we will limit the discussion and results in the rest of this paper to receiver antenna compensation only. Thus, for the specific purpose of this treatment, the true channel response is considered to be inclusive of the transmitter-side antenna distortion, and is given by

$$H_{th}(\theta_r, \phi_r, f) = H(\theta_t, \phi_t, \theta_r, \phi_r, f) A_t(\theta_t, \phi_t, f). \quad (8)$$

Our objective here is to estimate $H_{th}(\theta_r, \phi_r, f)$ given *a priori* knowledge of $A_r(\theta_r, \phi_r, f)$, as described below.

III. Compensation Algorithm

The transfer function of an antenna depends on its construction. The characterization of the antenna radiation pattern can be performed as a one-time operation, since the antenna properties remain constant as long as its construction and near-field environment are not subjected to any variations. The multipath DODs and DOAs, however, must be estimated continuously at run-time in a time-varying mobile environment.

For receiver-side antenna compensation, a spatial array consisting of identical antenna elements is used at the receiver for DOA estimation [14]. Whether the array is physical or synthetic does not affect the operational details of the antenna compensation scheme. This choice does, however, involve important practical considerations. A synthetic, or virtual, array can be reliably used only if the array synthesis duration is within the channel coherence time, which may render the approach impractical for fast-fading channels. A synthetic array is feasible in stationary environment, such as during indoor channel characterization measurements, as indeed will be the case in this paper (see Section IV-A). Besides reduced cost and hardware complexity, a major advantage of synthetic arrays is that antenna mutual coupling between array elements can be avoided. As is well known from antenna theory, mutual coupling can severely distort the far-field radiation pattern of an antenna, and can therefore invalidate the results [15]. For physical arrays, half-wavelength antenna separation must be ensured during array design to avoid mutual coupling [16].

With a rectangular array along the Cartesian axes, the antenna-distorted received signal at element location (x_r, y_r) can be represented by $R^{xy}_{thr}(f)$. This can be transformed to the angular-domain representation, $R_{thr}(f)$, using DOA estimation techniques. The Fourier method [17] offers a simple procedure, but does not provide the high angular resolution obtained with super-resolution techniques such as MUSIC, CLEAN, SAGE, or ESPRIT [14]. According to the Fourier method, we can write $R_{thr}(f) = \mathcal{F}_{xy}\{R^{xy}_{thr}(f)\}$, where $\mathcal{F}_{xy}$ denotes the two-dimensional spatial Fourier transform from the Cartesian to the spherical polar domain. Correspondingly, we will use $\mathcal{F}^{-1}_{xy}$ to denote the inverse transform.

Given the DOA information, the receiver-side antenna-compensated signal can be estimated from the received signal in the spherical polar coordinate system as

$$\hat{R}_{th}(\theta_r, \phi_r, f) = R_{thr}(f) A_r^{-1}(\theta_r, \phi_r, f) \quad (9)$$

where the estimation is considered accurate when the estimation error is small, i.e., $\left| R_{th}(\theta_r, \phi_r, f) - \hat{R}_{th}(\theta_r, \phi_r, f) \right| \to 0$.

If the compensation of both the transmit and the receive antennas is desired, it is straightforward to extend (9) to obtain an estimate, $\hat{H}$, of the true channel, given knowledge of the multipath DODs and DOAs, as shown by Fig. 1. Thus

$$\hat{R}_h(\theta_t, \phi_t, \theta_r, \phi_r, f) = A_t^{-1}(\theta_t, \phi_t, f) R_{thr}(f) A_r^{-1}(\theta_r, \phi_r, f)$$

from which the true channel estimate can be obtained as

$$\hat{H}(\theta_t, \phi_t, \theta_r, \phi_r, f) = S^{-1}(f) \hat{R}_h(\theta_t, \phi_t, \theta_r, \phi_r, f).$$

The process described by (9) is akin to zero-forcing equalization [18] of the antenna distortion in the space and frequency domains, and has low computational complexity, rendering runtime operation feasible. Note that, because of the inversion in (9), this process may be susceptible to noise enhancement, leading to erroneous, non-physical results. This situation can occur at angles where the antenna radiation pattern nulls or pseudo-nulls occur. Other, more complex estimation techniques, such as the minimum mean-squared error or maximum likelihood criteria, may be applied to remedy this potential problem [18]. The performance comparison of various candidate estimation techniques is, however, beyond the scope of the current paper. Also, many practical UWB antennas, including the discone antennas used for the experimental analysis in this paper, do not exhibit absolute nulls in their power radiation patterns.

This compensation process can also be described as a time-domain deconvolution. Thus, in the Cartesian space-time coordinate system, the receiver antenna compensated signal is $\hat{r}^{xy}_{th}(x_r, y_r, \tau) = \mathcal{F}^{-1}_{xy}\left\{\mathcal{F}^{-1}_{t}\left\{\hat{R}_{th}(\theta_r, \phi_r, f)\right\}\right\}$, where the

Fourier method has been used for space-to-angle transformation, and $\mathcal{F}_t^{-1}$ denotes the temporal inverse Fourier transform. When $s(t)$ is transmitted, the channel impulse response after receiver antenna compensation can be obtained as

$$\hat{h}_{th}^{xy}(x_r, y_r, \tau) = \mathcal{F}_t^{-1}\left\{S^{-1}(f)\hat{R}_{th}^{xy}(x_r, y_r, f)\right\}$$

where $\hat{R}_{th}^{xy}(x_r, y_r, f) = \mathcal{F}_t\{\hat{r}_{th}^{xy}(x_r, y_r, \tau)\}$.

Now, as $\hat{R}_{th}^{xy}$ is a UWB signal spanning bandwidth W, its corresponding wideband angular power spectrum (APS), $\hat{\mathcal{R}}_{th}$, can be obtained by power integration in the angular domain across the constituent frequency components. Mathematically

$$\hat{\mathcal{R}}_{th}(\theta_r, \phi_r) = \int_W |\hat{R}_{th}(\theta_r, \phi_r, f)|^2 df \tag{10}$$

and similarly for the other quantities in the above discussion.

IV. Performance Evaluation

We now apply the proposed compensation technique to measured UWB channel data, distorted by real antennas, and evaluate its efficacy in terms of various metrics related to localization accuracy and channel fading statistics.

A. Experimental Configuration

Indoor channel measurements are conducted in the frequency domain with the help of a vector network analyzer (VNA) over the 3.1–10.6 GHz UWB band. End-to-end calibration of the equipment, including the VNA, cables, connectors and amplifiers, but not the antennas, is performed prior to conducting the measurements. A horizontal receiver array is synthesized by means of an automated rectangular positioning grid. Thus 10 000 complex channel realizations are measured in a 1 m $\times$ 1 m region, with 1 cm spatial resolution. The stationarity of the environment, a necessary condition for the validity of the antenna array synthesis procedure, is ensured by means of physical isolation, as demonstrated in [19]. A representative channel measurement configuration is illustrated in Fig. 3. As shown, the measurement environment consists of a small office room, with a number of scattering objects. The distance of the transmitter and the center of the receiving grid in this measurement is 4.5 m, and the antennas are at a height of 1.5 m. The measurement process is repeated in multiple indoor environments for statistical verification of the results.

For channel measurement, vertically polarized discone antennas with identical construction are used [5]. The antenna power radiation pattern is measured at various frequencies within the spectral range of interest inside the anechoic chamber. The antenna transfer function magnitude is obtained from the power radiation pattern as $A_i(\theta_i, \phi_i, f) = \sqrt{P_i(\theta_i, \phi_i, f)}$, for $i = \{t, r\}$. The results in this section are based on the antenna transfer function magnitude compensation, neglecting the phase component. This approach is valid if $\angle A_i(\theta_i, \phi_i, f)$ varies linearly with f, or in other words, the group delay does not depend on f. The antennas under consideration satisfy this condition, as shown experimentally in [20].

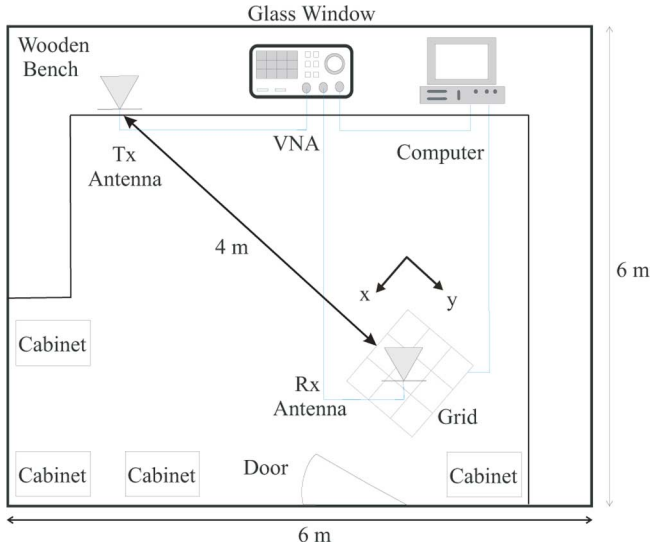

Fig. 3. Indoor measurement environment and experimental configuration.

B. Average Power Delay Profile

The local average power delay profile (APDP) of the UWB channel can be evaluated as

$$p_{av}(\tau) = \int_{-X/2}^{X/2}\int_{-Y/2}^{Y/2} |\hat{h}_{th}^{xy}(x_r, y_r, \tau)|^2 dxdy$$

where (X, Y) defines the span of a local spatial region in the two-dimensional Cartesian coordinate system, and is taken as 1 m^2 in this paper. The power normalization

$$\int_0^{\tau_{\max}} \left|\hat{h}_{th}^{xy}(x_r, y_r, \tau)\right|^2 dt = 1$$

is applied to each channel impulse response before evaluating the APDP to remove small-scale fading and large-scale pathloss effects. In the above relation, $\tau_{\max}$ represents the maximum excess delay of the channel.

Fig. 4 shows the APDP of the UWB channel without and with receiver-side antenna compensation. Some additional multipath components and clusters become visible in Fig. 4(b), which are otherwise masked due to the receive antenna radiation pattern. The most prominent cluster that appears only after the compensation occurs at $\tau \approx 45$ ns. Due to the reduction in the waveform dispersion for each individual MPC, the multipath resolution is also increased. The reason is that the effective bandwidth of the composite channel, reduced due to the antenna's spatio-spectral filtering [5], is partially restored by compensation, in turn enhancing the time-resolution.

C. Sensor Localization

Many localization schemes, based on the detection of the dominant multipath DOA, use an estimate of the angle of the signal source to calculate its spatial location. It is obvious that accurate estimation of the DOA is critical for such a localization scheme. For our measurements, the DOA information is contained in $\hat{R}_{th}^{xy}(x_r, y_r, f)$, and can be extracted by conversion to $\hat{R}_{th}(\theta_r, \phi_r, f)$. This information, however, is corrupted by the

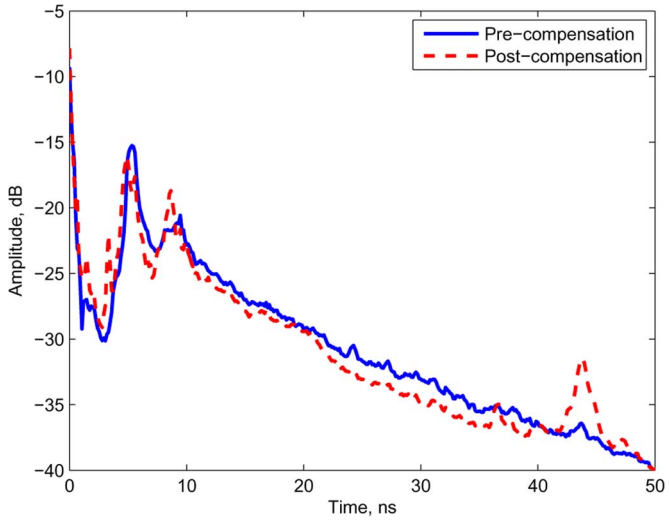

Fig. 4. The local average power delay profile of the LOS UWB channel.

antenna effects, with the possibility of a certain error in estimating the source direction.

Fig. 5 shows the angular power spectra of the pre- and post-compensation channels. Due to the experimental conditions, the true line-of-sight (LOS) component is incident at $(\theta, \phi) = (90°, 0°)$. In the pre-compensated radio image of the channel, however, two strong arrivals appear at (45°, 0°) and (80°, 0°), where the latter corresponds to an approximation of the true LOS direction.[1] The multipath component arriving after a single reflection from the ceiling, incident at (45°, 0°), is artificially emphasized due to the antenna's high gain in the oblique direction. An elliptical distortion is also observed in the image, elongating the multipath clusters along the zenith axis. After antenna compensation, this elliptical distortion is significantly diminished, in turn reducing the estimation ambiguity. It also shows that the now dominant (80°, 0°) signal is the true maximum and the LOS direction can now be more clearly identified. Also, some of the incident multipath energy from the top corner of the room is now visible. Thus the uncertainty in the DOA, and hence source localization, due to the antenna's selective enhancement of some paths has been alleviated. The direction of the transmitting terminal can now be determined with improved accuracy.

D. SNR Degradation

Simple linear equalization of the antenna distortion function can possibly lead to some noise enhancement, incurring an SNR penalty. We now quantify this SNR degradation from our measured channel responses using a semianalytical approach. We consider a communications system that uses multicarrier modulation, such as orthogonal frequency-division multiplexing (OFDM), with per-tone single-tap zero-forcing channel equalization, in accordance with [21]. We assume that the cyclic prefix is longer than the channel delay spread so that

[1]Note that the transmitter and receiver lie in the same horizontal plane in our experimental setup, and therefore, strictly speaking, the true LOS direction is (90°, 0°). However, a planar array is inherently incapable of steering its beam along its plane, with a consequent shift from the true zenith DOA, so that the estimation error $\delta\theta = |90° - \theta| > 0$.

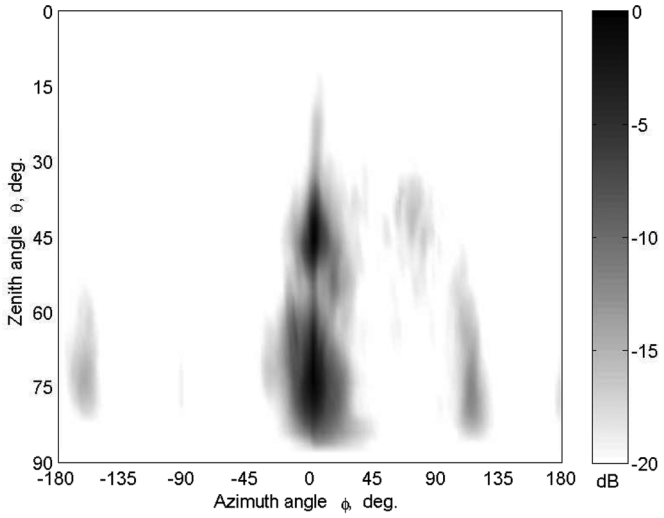

(a) Before compensation

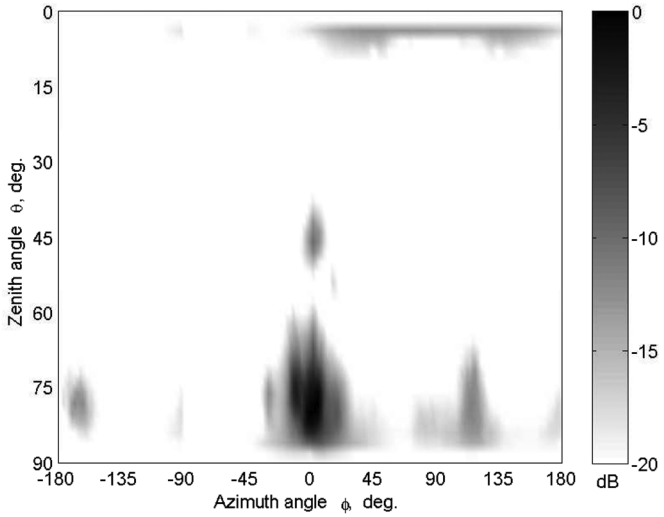

(b) After compensation

Fig. 5. The multipath angular power spectra of the indoor line-of-sight (LOS) UWB channel. The transmitter is located at $(\theta, \phi) = (90°, 0°)$. The spectra are normalized with respect to the maximum intensity and thresholded to 20 dB below it.

no intersymbol interference (ISI) occurs. In this treatment, we consider the uncoded bit-error rate (BER) of the system for a binary antipodal signaling scheme. Then the instantaneous probability of error for a given discrete-time power-normalized channel impulse response, h_n, is given by

$$P_e(h_n) = \frac{1}{K}\sum_{k=1}^{K} Q\left(\sqrt{2\gamma|H_k|^2}\right)$$

where $H_k = \mathcal{F}_t\{h_n\}$ is the complex channel gain at the k^{th} discrete frequency component, $Q(\cdot)$ is the Marcum-Q function, $\gamma = E_b/N_0$ is the SNR, E_b is the bit energy, and N_0 is the noise power spectral density. This reception scheme is suboptimal in that, in the absence of channel coding, it approaches but does not achieve the matched filter bound for a flat-fading Rayleigh channel [18]. It is, however, sufficient for the pre- and post-compensation channel comparison in this paper. We randomly select

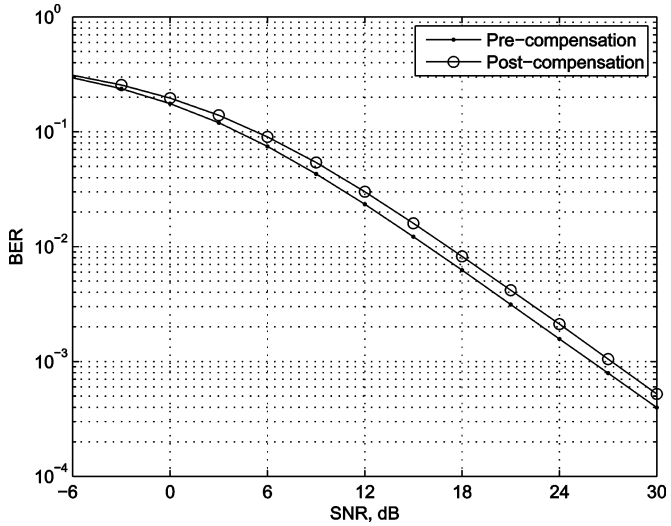

Fig. 6. The bit-error probability (BER) as a function of the signal-to-noise ratio (SNR). An SNR penalty may be incurred on antenna compensation due to angular noise enhancement at the antenna radiation pattern nulls.

1000 channel realizations from the measurement ensemble for the error probability evaluation.

The mean BER of the system before and after antenna compensation is shown in Fig. 6. The SNR degradation due to compensation is found to be less than 1 dB for our measurements. The results will vary to an extent with other antennas or propagation environments. However, the indoor office environment and omnidirectional antennas used in our analysis represent a typical operating scenario for an indoor wireless network, and the general results are therefore useful.

E. Small-Scale Fade Mitigation

An important design objective for wireless communications systems is the reduction in small-scale fading and spatial variability of the channel. We now show that the antennas contribute to this fading, and removing their effects thus reduces the spatial variation. For this purpose, we consider the values of the mean excess delay, τ_{mean}, and the maximum excess delay, $\tau_{\max}$, extracted from the local ensemble of channel responses measured over a $1\mathrm{m}^2$ region. The definitions of these delay spread parameters can be found in [22].

Fig. 7 shows the spatial variation of τ_{mean} with and without antenna compensation. Fig. 7(a) shows the interference pattern formed due to multipath. In Fig. 7(b), however, ignoring the edges, the variation is reduced considerably, and a lower mean value is obtained. Similar behavior can be observed for $\tau_{\max}$ from Fig. 8, including increased spatial uniformity and reduction in small-scale variability. Note that the edge effects in Figs. 7 and 8 arise as a spatial filtering artifact. This is due to the specific radiation pattern having increased the amplitude of higher spatial frequency components in the far-field plane.

F. Delay Spread Compression

The channel delay spread is inversely related to the achievable data-rate, and is therefore of fundamental importance in communications system design. Therefore we next consider the statistics of the channel delay spread before and after antenna

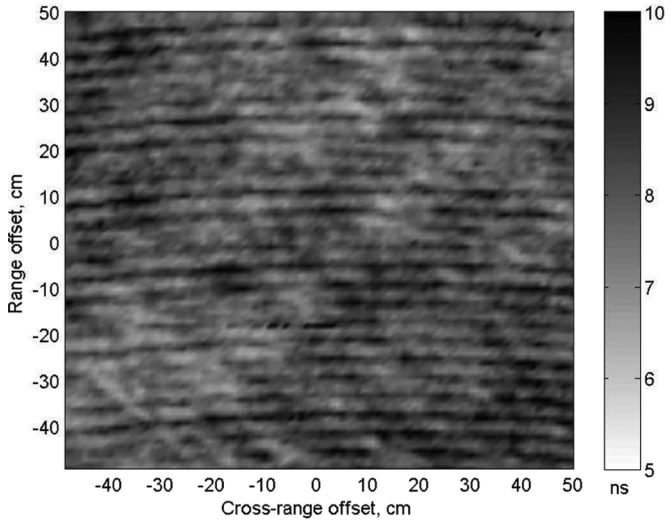

(a) Before compensation

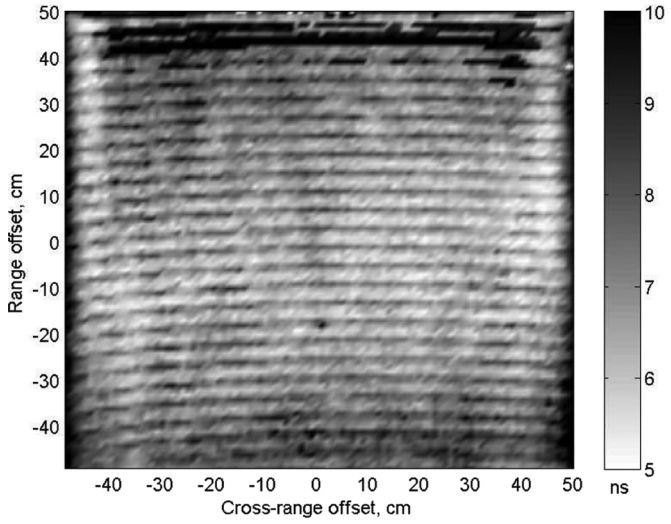

(b) After compensation

Fig. 7. The spatial variation of the multipath mean excess delay.

compensation. The cumulative distribution functions (CDFs) of the mean and maximum excess delay are estimated from the local channel measurement ensemble. In order to avoid the edge effects in the post-compensation channel responses, we exclude the channels that lie close to the periphery of the planar measurement region. Thus we consider only $h_{thr}^{xy}(x_r', y_r', t)$ and $\hat{h}_{th}^{xy}(x_r', y_r', t)$ for this analysis, where $-X'/2 \leq x_r' \leq X'/2$ and $-Y'/2 \leq y_r' \leq Y'/2$, such that $(x_r, y_r) - (x_r', y_r')$ defines the points in the peripheral region of the Cartesian-domain channel measurement, where we have assumed the center of the receiving grid to lie at the origin of the coordinate system. By an inspection of the $1\ \mathrm{m}^2$ spatial patterns in Figs. 7 and 8, a 0.1 m wide peripheral band is found suitable to exclude the edges from the statistical analysis.

Fig. 9 shows the mean and maximum delay spread CDFs thus obtained. The mean excess delay has an average value of 8 ns before compensation, which falls to 6.7 ns after compensation. Similarly, the maximum excess delay is reduced by 3 ns due to compensation. In addition, the variance of the maximum excess delay distribution is reduced considerably, as evident from the

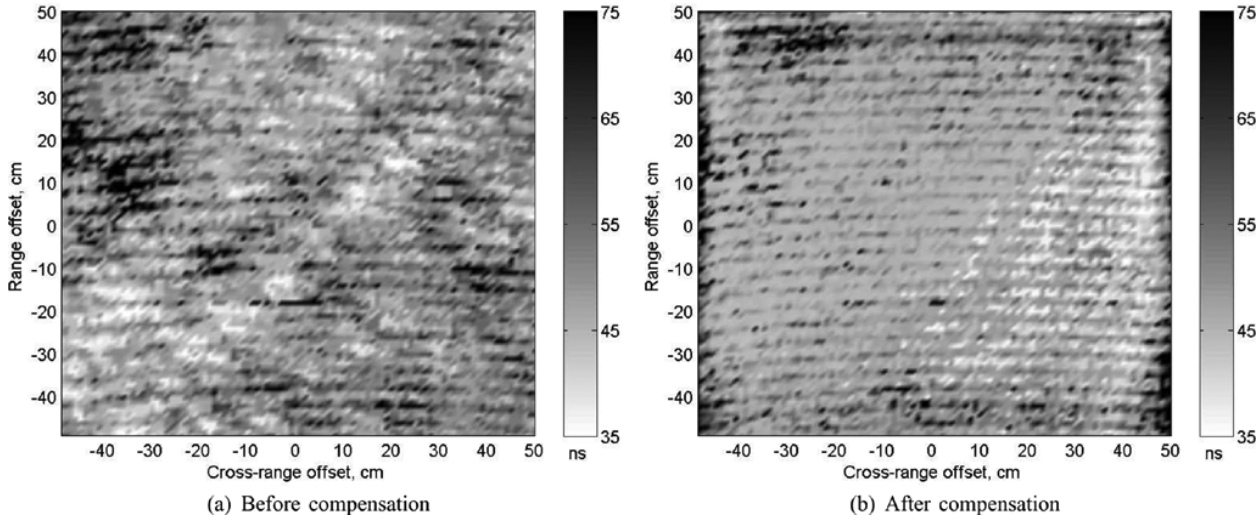

Fig. 8. The spatial variation of the multipath maximum excess delay.

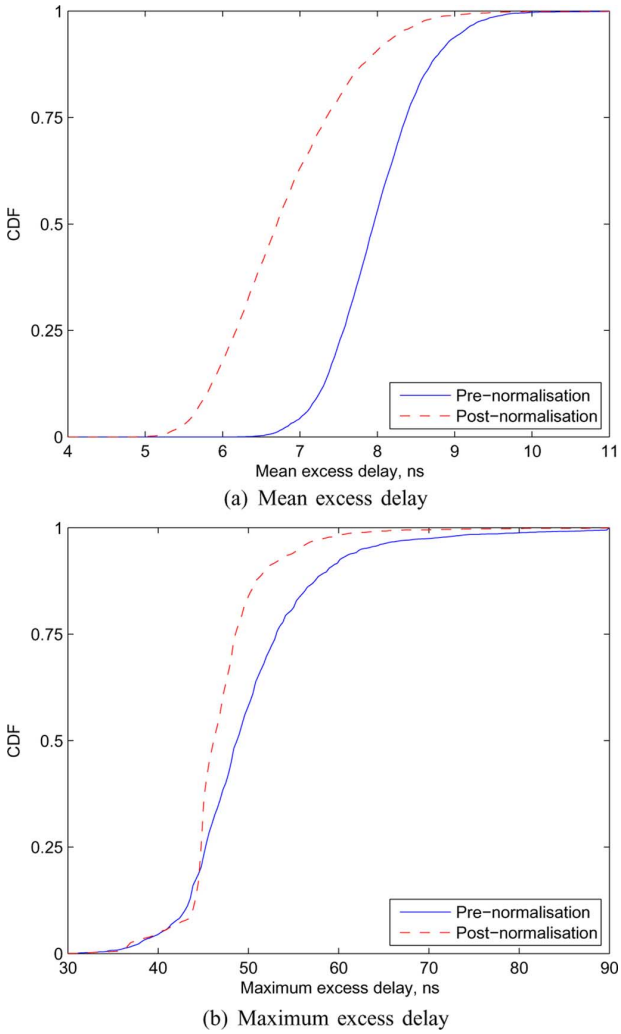

Fig. 9. Cumulative distribution functions (CDFs) of the UWB indoor channel's pre- and post-compensation delay statistics.

straightening of the post-compensation CDF in the figure, indicating decreased small-scale spatial variability of the channel. This delay spread reduction quantifies the channel dispersion mitigation achieved by antenna compensation.

V. Conclusion

This paper has discussed an antenna array based scheme for mitigating the channel distortion introduced by the antennas. The wideband equalization of the antenna radiation pattern can provide a quasi-isotropic reconstruction of the propagation channel. The DOA estimation results in this paper have shown that antenna compensation of this type can remove antenna-based source localization ambiguities, thus significantly enhancing the performance of the localizing sensors. The spectral anisotropy of a typical UWB antenna also reduces the effective channel bandwidth and increases the delay spread. Antenna compensation leads to a reduction in the spatial small-scale fading and temporal dispersion introduced by antennas. As the channel delay spread and the achievable data rate are directly related, this delay spread compression translates into an increase in the achievable information rate. This performance improvement in localization estimation and reduction in spatial variability does, however, incur an SNR penalty, which is an inherent problem of the technique; in our measurements, the SNR degradation is found to be about 1 dB. Our analysis has demonstrated that the distortion due to the antennas can be substantial for UWB systems, significantly affecting the channel characteristics and consequently the link performance. UWB antennas with spatio-spectrally uniform radiation characteristics pose a considerable design challenge, especially considering the cost and size constraints of elements for wireless sensors and handsets. Antenna distortion compensation can, however, be used effectively to mitigate the shortcomings of a nonideal UWB antenna.

References

[1] B. Allen, M. Dohler, E. E. Okon, W. Q. Malik, A. K. Brown, and D. J. Edwards, Eds., *Ultra-Wideband Antennas and Propagation for Communications, Radar and Imaging*. London, U.K.: Wiley, 2006.

[2] "Revision of Part 15 of the Commission's Rules Regarding Ultra-Wideband Transmission Systems: First Report and Order," Federal Communications Commission, Washington, DC, 2002, Tech. Rep. FCC 02–48.
[3] A. F. Molisch, "Ultrawideband propagation channels—Theory, measurement, and modeling," *IEEE Trans. Veh. Technol.*, vol. 54, pp. 1528–1545, Sep. 2005.
[4] H. G. Schantz, *The Art and Science of Ultra-Wideband Antennas*. Boston, MA: Artech House, 2005.
[5] W. Q. Malik, D. J. Edwards, and C. J. Stevens, "Angular-spectral antenna effects in ultra-wideband communications links," *Proc. Inst. Elect. Eng. Commun.*, vol. 153, no. 1, pp. 99–106, Feb. 2006.
[6] H. G. Schantz, "Dispersion and UWB antennas," presented at the IEEE Int. Workshop on Ultra Wideband Systems Joint with Conf. Ultrawideband Systems and Technology, Kyoto, Japan, May 18–21, 2004.
[7] W. Sörgel and W. Wiesbeck, "Influence of the antennas on the ultra-wideband transmission," *EURASIP J. Applied Sig. Proc.*, vol. 2005, no. 3, pp. 296–305, Mar. 2005.
[8] M. Ghavami, L. Michael, and R. Kohno, *Ultra Wideband Signals and Systems in Communication Engineering*, 2nd ed. London, U.K.: Wiley, 2007.
[9] S. Gezici, Z. Tian, G. B. Giannakis, H. Kobayashi, A. F. Molisch, H. V. Poor, and Z. Sahinoglu, "Localization via ultra-wideband radios: A look at positioning aspects for future sensor networks," *IEEE Signal Proc. Mag.*, vol. 22, no. 4, pp. 70–84, Jul. 2005.
[10] W. Q. Malik, D. J. Edwards, Y. Zhang, and A. K. Brown, "Three-dimensional equalization of ultrawideband antenna distortion," presented at the Proc. Int. Conf. Electromagnetics in Advanced Applications (ICEAA), Torino, Italy, Sep. 17–21, 2007.
[11] I. M. Pinto, V. Galdi, and L. B. Felsen, Eds., *Electromagnetics in a Complex World*. Heidelberg, Germany: Springer, 2004.
[12] A. Shlivinski, A. Heyman, and R. Kastner, "Antenna characterization in the time domain," *IEEE Trans. Antennas Propag.*, vol. 45, pp. 1140–1149, Jul. 1997.
[13] W. Q. Malik and A. F. Molisch, "Ultrawideband antenna arrays and directional propagation channels," in *Proc. Eur. Conf. Antennas Propagation (EuCAP)*, Nice, France, Nov. 6–10, 2006.
[14] S. Haykin, *Array Signal Processing*. Englewood Cliffs, NJ: Prentice Hall, 1985.
[15] G. Kotyrba and H. J. Chaloupka, "On signal distortion in compact UWB arrays due to element interaction," presented at the Proc. IEEE Antennas Propagation Soc. Int. Symp., Washington, DC, Jul. 3–8, 2005.
[16] J. W. Wallace and M. A. Jensen, "Mutual coupling in MIMO wireless systems: A rigorous network theory analysis," *IEEE Trans. Wireless Commun.*, vol. 3, no. 4, pp. 1317–1325, Jul. 2004.
[17] E. Hecht and A. Zajac, *Optics*, 4th ed. London, U.K.: Addison-Wesley, 2001.
[18] G. L. Stüber, *Principles of Mobile Communications*, 2nd ed. Norwell, MA: Kluwer, 2001.
[19] W. Q. Malik and D. J. Edwards, "Measured MIMO capacity and diversity gain with spatial and polar arrays in ultrawideband channels," *IEEE Trans. Commun.*, vol. 55, pp. 2361–2370, Dec. 2007.
[20] W. Q. Malik, C. J. Stevens, and D. J. Edwards, "Spatio-spectral normalisation for ultra wideband antenna dispersion," presented at the IEEE High Frequency Postgraduate Student Colloquim, Manchester, U.K., Sep. 6–7, 2004.
[21] A. Batra, J. Balakrishnan, A. Dabak, R. Gharpurey, J. Lin, P. Fontaine, J.-M. Ho, S. Lee, M. Frechette, S. March, and H. Yamaguchi, Multi-band OFDM Physical Layer Proposal for IEEE 802.15 Task Group 3a IEEE, 2003, Tech. Rep. P802.15–03/268r0-TG3a.
[22] T. S. Rappaport, *Wireless Communications: Principles and Practice*, 2nd ed. Englewood Cliffs, NJ: Prentice Hall, 2001.

Wasim Q. Malik (S'97–M'05) received the B.E. degree from the National University of Sciences and Technology, Pakistan, in 2000, and the D.Phil. degree from the University of Oxford, U.K., in 2005, both in electrical engineering.

Since 2007, he has been with the Massachusetts Institute of Technology, Cambridge, where he is a Postdoctoral Fellow. From 2005 to 2007, he was a Research Fellow at the University of Oxford and a Junior Research Fellow in Science at Wolfson College, Oxford. He is an Editor of the book *Ultra-Wideband Antennas and Propagation for Communications, Radar and Imaging* (U.K.: Wiley, 2006). He routinely serves on the organizing and technical program committees of various international conferences. He has published in excess of 70 papers in refereed journals and conferences.

Dr. Malik received the ESU Lindemann Science Fellowship in 2007, the Best Paper Award from the ARMMS RF and Microwave Conference (Steventon, U.K., 2006), and Recognition of Service Award from the Association for Computing Machinery (ACM) in 2000. He is a member of the Society for Neuroscience.

Christopher J. Stevens read physics at the University of Oxford, Oxford, U.K., graduating in 1990 where he received the D.Phil. degree in condensed matter physics from the University of Oxford, in 1994.

He has worked for the European Union Human Capital Mobility scheme at the Universita degli Studi di Lecce. He then moved back to Oxford for a three-year postdoctoral position studying the physics of novel superconducting materials. In 1997, he received a Royal Academy of Engineering Senior Research Fellowship and moved disciplines to engineering. He now holds an engineering faculty position at the University of Oxford and is a Fellow of St. Hugh's College, Oxford.

Dr. Stevens is a member of the Institution of Engineering and Technology (IET), London, U.K., and a founder member of the VORTEX consortium.

David J. Edwards received the B.Sc. degree in physics in 1973, the M.Sc. degree in physics of materials in 1974, and the Ph.D. degree in engineering in 1987, all from Bristol University, Bristol, U.K.

He is currently a Professor of engineering science at the University of Oxford, Oxford, U.K., and a Fellow of Wadham College, Oxford. After a period of 12 years working at British Telecom, he has been an academic for 21 years. He has acted as a Consultant to a large number of industrial organizations. He has been awarded a number of patents and several have appeared as licensed commercial products. He has a strong record of innovation in communications systems, techniques and technologies and has published in excess of 300 papers.

Dr. Edwards is a Fellow of the Institution of Engineering and Technology (IET), London, U.K., and the Royal Astronomical Society. He has received a number of awards and prizes for his work and has been extremely well supported by funding from research councils, industry and government agencies. He has served on several national and international committees relating to antennas and propagation.